 CMES, vol.34, no.2, pp.137-154, 2008

A Topology Optimization Design for the Continuum Structure Based on the Meshless Numerical Technique

Zheng Juan[1,2,3], Long Shuyao[1,2], Xiong Yuanbo[1,2] and Li Guangyao[1]

Abstract: In this paper, the meshless radial point interpolation method (RPIM) is applied to carry out a topology optimization design for the continuum structure. Considering the relative density of nodes as a design variable, and the minimization of compliance as an objective function, the mathematical formulation of the topology optimization design is developed using the SIMP (solid isotropic microstructures with penalization) interpolation scheme. The topology optimization problem is solved by the optimality criteria method. Numerical examples show that the proposed approach is feasible and efficient for the topology optimization design for the continuum structure, and can effectively overcome the checkerboard phenomenon.

Keyword: radial point interpolation method (RPIM); topology optimization design for continuum structure; SIMP; optimality criteria method; checkerboard phenomenon

1 Introduction

Topology optimization design for the continuum structures is one of the most challenging research topics in the field of the structural optimization [Bendsoe and Sigmund (2003)]. The purpose of the topology optimization design is to find the optimal lay-out of a structure within a specified region. In this problem the only known quantities are the applied loads, the possible support conditions, the volume of the structure to be constructed and possibly some additional design restrictions, and the physical size and the shape of the structure are unknown. The topology optimization design for the continuum structures is essentially a discretized 0-1 variables problem. Recently, with the increase of interest in this field, various models and methods for structural topology optimization were explored, with

[1] State Key Laboratory of Advanced Design and Manufacture for Vehicle Body, Hunan University, Changsha, China
[2] College of Mechanics and Aerospace Engineering, Hunan University, Changsha, China
[3] Corresponding author. Tel.: +86-0731-8824724. E-mail: dingdang8209@163.com

goals of improving the computational efficiency, and alleviating numerical instabilities [Cisilino (2006), Li and Atluri (2008a,b), Michael and Wang (2004), Michael and Zhou (2004), Tapp, Hansel, Mittelstedt and Becker (2004), Wang and Wang (2006), Wang, Lim, Khoo and Wang (2007a, b, c, 2008), Zhou and Wang(2006)]. For the topology optimization design for the continuum structures, homogenization approach [Bendsoe and Kikuchi (1988)], variable density approach [Bendsoe and Sigmund (1999)] and evolutionary structural optimization (ESO) approach [Zhou and Rozvany (2001)] are often employed. In the variable density approach, a density function $\rho(x)$, which varies continuously between 1 and 0 with density 1 characterizing the material and 0 the void (no material), is introduced to represent the material distribution in the design domain. Solid isotropic microstructures with penalizetion (SIMP) [Bendsoe and Sigmund (1999)] and rational approximation of material properties (RAMP) [Stolpe and Svanberg (2001)] are two common density interpolation models.

To date, the numerical method prevailing in topology optimization design is the finite element method (FEM). However, FEM has a big limitation continuously remeshing the finite element model when dealing with large deformation or moving boundary problems. Meshless methods have been achieved remarkable progress in recent years, such as smooth particle hydrodynamics method (SPH) [Monaghan (1992)], element-free Galekin method (EFG) [Belytschko and Lu et al. (1994)], meshless local Petrov-Galekin method (MLPG) [Atluri and Zhu (1998)]. The meshless methods use a set of nodes scattered within the problem domain and on boundaries of the domain. These nodes do not form a mesh meaning it does not need any information on the relationship between nodes for the interpolation of the unknown field variables. Since no element connectivity data is required, the remeshing characteristic of FEM is avoided. Liu and Gu (2001) proposed the meshless point interpolation methods (PIM) based on the Galekin weak form. However, in PIM, as polynomial basis functions are used, the interpolation moment matrix can be singular. As an interpolation scheme, radial basis functions (RBF) are becoming more and more attractive in meshless methods. In Raju, Phillips and Krishnamurthy (2004), they adopt the RBF as the trial function in the MLPG formulation for beam problems. The major advantage of radial PIM (RPIM) is that its shape functions possess the Kronecker Delta function property, which allows simple enforcement of essential boundary conditions, and using RBF can effectively solve the singularity problem of the polynomial PIM. Therefore, RPIM is currently used more widely than the polynomial PIM. RPIM has been successfully applied to 2D and 3D solid mechanics [Liu and Gu (2001); Liu and Zhang et al. (2005)], plate and shell structures [Liu and Liu et al. (2002)], problems of smart materials [Liu and Dai et al. (2003)], material non-linear problems in civil engineering [Wang et

al. (2002)], and so on.

In this paper, the topology optimization design for the continuum structures is formulated using the meshless radial point interpolation method for two-dimensional elastostatics problems. Considering the relative density of nodes as a design variable, the proposed method effectively eliminates the checkerboard phenomenon. Finally, the feasibility and efficiency of the proposed method are illustrated with several 2D examples that are widely used in the topology optimization design.

2 Meshless radial point interpolation method for plane elasticity

2.1 RPIM shape function

Consider an approximation function for a field variable $u(\mathbf{x})$ in a domain. The function $u(\mathbf{x})$ can be approximated by using a radial basis function with a polynomial basis function as

$$u(\mathbf{x}) = \sum_{i=1}^{n} R_i(\mathbf{x}) a_i + \sum_{j=1}^{m} P_j(\mathbf{x}) b_j = \mathbf{R}^{\mathrm{T}}(\mathbf{x})\mathbf{a} + \mathbf{P}^{\mathrm{T}}(\mathbf{x})\mathbf{b} \tag{1}$$

where $R_i(\mathbf{x})$ is a radial basis function (RBF), a_i is the coefficient for $R_i(\mathbf{x})$, $P_j(\mathbf{x})$ is monomial in the space coordinates $\mathbf{x}^{\mathrm{T}} = [x,\ y]$, b_j is the coefficient for $P_j(\mathbf{x})$, n is the number for RBF, m is the number for the polynomial basis function, usually $m \ll n$. For two-dimensional problems, the linear basis functions are given by $\mathbf{P}^{\mathrm{T}}(\mathbf{x}) = [1, x, y]$.

Using RBF can effectively overcome the singularity problem of the PIM based on only polynomial basis function. There are four often used RBFs as follows

1) Multi-quadrics (MQ)

$$R_i(x,y) = \left(r_i^2 + (\alpha_c d_c)^2\right)^q \quad \alpha_c \geq 0$$

2) Gaussian (EXP)

$$R_i(x,y) = \exp\left[-\alpha_c \left(\frac{r_i}{d_c}\right)^2\right]$$

3) Thin Plate Spline (TPS)

$$R_i(x,y) = r_i^{\eta}$$

4) Logarithmic

$$R_i(x,y) = r_i^{\eta} \log r_i$$

where $r_i = \sqrt{(x-x_i)^2+(y-y_i)^2}$ is a distance between interpolating point (x,y) and the node (x_i,y_i), α_c, q, η are shape parameters, d_c is a characteristic length that relates to the nodal spacing in the local support domain of the point of interest x, and it is usually the average nodal spacing for all the nodes in the local support domain.

In order to determine the coefficients a_i and b_j in Equation (1), a support domain is formed for the point of interest x, and n field nodes are included in the support domain. Coefficients a_i and b_j in Equation (1) can be determined by enforcing Equation (1) to be satisfied at these n nodes surrounding the point of interest x, which leads to a set of n equations.

The interpolation at the kth node has

$$u_k = u(x_k,y_k) = \sum_{i=1}^{n} R_i(x_k,y_k)\,a_i + \sum_{j=1}^{m} P_j(x_k,y_k)\,b_j \quad k = 1,2,...,n \tag{2}$$

The matrix form of these equations can be expressed as

$$\mathbf{U_s} = \mathbf{R_0 a} + \mathbf{P_m b} \tag{3}$$

However, there are $n+m$ variables in Equation (3). The additional m equations can be added using the following m constraint conditions.

$$\sum_{i=1}^{n} P_j(x_i,y_i)\,a_i = \mathbf{P}_m^{\mathrm{T}}\mathbf{a} = 0,\ j = 1,2,\ldots,m \tag{4}$$

Combing Equations (3) and (4), we can obtain

$$\overline{\mathbf{U}}_s = \begin{Bmatrix} \mathbf{U}_s \\ 0 \end{Bmatrix} \begin{bmatrix} \mathbf{R}_0 & \mathbf{P}_m \\ \mathbf{P}_m^{\mathrm{T}} & 0 \end{bmatrix} \begin{Bmatrix} \mathbf{a} \\ \mathbf{b} \end{Bmatrix} = \mathbf{G} \begin{Bmatrix} \mathbf{a} \\ \mathbf{b} \end{Bmatrix} \tag{5}$$

Equation (1) can be re-written as

$$u(\mathbf{x}) = \mathbf{R}^{\mathrm{T}}(\mathbf{x})\,\mathbf{a} + \mathbf{P}^{\mathrm{T}}(\mathbf{x})\mathbf{b} = \begin{bmatrix} \mathbf{R}^{\mathrm{T}}(\mathbf{x}) & \mathbf{P}^{\mathrm{T}}(\mathbf{x}) \end{bmatrix} \begin{Bmatrix} \mathbf{a} \\ \mathbf{b} \end{Bmatrix} \tag{6}$$

Using Equation (5), we can obtain

$$u(\mathbf{x}) = \begin{bmatrix} \mathbf{R}^{\mathrm{T}}(\mathbf{x}) & \mathbf{P}^{\mathrm{T}}(\mathbf{x}) \end{bmatrix} \mathbf{G}^{-1} \overline{\mathbf{U}}_{\mathbf{s}} = \overline{\mathbf{\Phi}}^{\mathrm{T}}(\mathbf{x})\,\overline{\mathbf{U}}_{\mathbf{s}} \tag{7}$$

where $\overline{\mathbf{\Phi}}^{\mathrm{T}}(\mathbf{x})$ is the shape functions of the RPIM and can be expressed as

$$\begin{aligned} \overline{\mathbf{\Phi}}^{\mathrm{T}}(\mathbf{x}) &= \begin{bmatrix} \mathbf{R}^{\mathrm{T}}(\mathbf{x}) & \mathbf{P}^{\mathrm{T}}(\mathbf{x}) \end{bmatrix} \mathbf{G}^{-1} \\ &= \begin{bmatrix} \phi_1(\mathbf{x}) & \phi_2(\mathbf{x}) & \cdots & \phi_n(\mathbf{x}) & \phi_{n+1}(\mathbf{x}) & \cdots & \phi_{n+m}(\mathbf{x}) \end{bmatrix} \end{aligned} \tag{8}$$

Finally, the shape functions of the RPIM corresponding to the nodal displacement vector $\Phi(\mathbf{x})$ are obtained as

$$\Phi^{\mathrm{T}}(\mathbf{x}) = [\phi_1(\mathbf{x}) \ \phi_2(\mathbf{x}) \ \cdots \ \phi_n(\mathbf{x})] \tag{9}$$

2.2 Discrete Equations of 2D plane problem [Liu and Gu (2004)]

Consider the following standard two-dimension problem of linear elasticity defined in the domain Ω and bounded by Γ

$$\begin{cases} \mathbf{L}^{\mathrm{T}}\boldsymbol{\sigma} + \mathbf{b} = 0 & \in \Omega \\ \boldsymbol{\sigma}\mathbf{n} = \overline{\mathbf{t}} & \in \Gamma_t \\ \mathbf{u} = \overline{\mathbf{u}} & \in \Gamma_u \end{cases} \tag{10}$$

where $\boldsymbol{\sigma}$ is the stress tensor, which corresponds to the displacement field $\mathbf{u}$, $\mathbf{b}$ is a body force vector, $\mathbf{L}$ is differential operator defined by

$$\mathbf{L} = \begin{bmatrix} \frac{\partial}{\partial x} & 0 \\ 0 & \frac{\partial}{\partial y} \\ \frac{\partial}{\partial y} & \frac{\partial}{\partial x} \end{bmatrix}$$

$\overline{\mathbf{t}}$ is the prescribed traction on the natural boundaries, $\overline{\mathbf{u}}$ is the prescribed displacement on the essential boundaries, $\mathbf{n}$ is the vector of unit outward at a point on the natural boundary.

The variational form of Equation (10) is posed as follows

$$\int_{\Omega} (\mathbf{L}\delta\mathbf{u})^{\mathrm{T}} (\mathbf{D}\mathbf{L}\mathbf{u}) \, \mathrm{d}\Omega - \int_{\Omega} \delta\mathbf{u}^{\mathrm{T}}\mathbf{b} \mathrm{d}\Omega - \int_{\Gamma_t} \delta\mathbf{u}^{\mathrm{T}}\overline{\mathbf{t}} \mathrm{d}\Gamma = 0 \tag{11}$$

In order to obtain the discretized system equations, the problem domain Ω and its boundary Γ are represented by properly distributed field nodes. Using the shape functions of the RPIM the displacement at any point x can be approximated as

$$\mathbf{u}^h = \begin{Bmatrix} u \\ v \end{Bmatrix} = \begin{bmatrix} \phi_1 & 0 & \cdots & \phi_n & 0 \\ 0 & \phi_1 & \cdots & 0 & \phi_n \end{bmatrix} \begin{Bmatrix} u_1 \\ v_1 \\ \vdots \\ u_n \\ v_n \end{Bmatrix} = \boldsymbol{\Phi}\mathbf{u} \tag{12}$$

where $\boldsymbol{\Phi}$ is the matrix of the shape functions, $\mathbf{u}$ is the vector of the displacements at the field nodes in the support domain, and n is the number of nodes in the support domain of a interest point at x.

Equation (12) can also be written in the following form of nodal summation.

$$\mathbf{u}^h = \sum_I^n \begin{bmatrix} \phi_I & 0 \\ 0 & \phi_I \end{bmatrix} \begin{Bmatrix} u_I \\ v_I \end{Bmatrix} = \sum_I^n \mathbf{\Phi}_I \mathbf{u}_I \tag{13}$$

where $\mathbf{\Phi}_I$ is the matrix of shape functions of node I, and $\mathbf{u}_I$ is the nodal displacements.

From Equation (13), we can obtain

$$\delta\mathbf{u}^h = \mathbf{\Phi}\delta\mathbf{u} = \sum_I^n \mathbf{\Phi}_I \delta\mathbf{u}_I \tag{14}$$

Using strain-displacement equations and the approximated displacements, the strains can be obtained as

$$\boldsymbol{\varepsilon} = \mathbf{L}\mathbf{u}^h = \mathbf{L}\Phi\mathbf{u} = \begin{bmatrix} \frac{\partial}{\partial x} & 0 \\ 0 & \frac{\partial}{\partial y} \\ \frac{\partial}{\partial y} & \frac{\partial}{\partial x} \end{bmatrix} \begin{bmatrix} \phi_1 & 0 & \cdots & \phi_n & 0 \\ 0 & \phi_1 & \cdots & 0 & \phi_n \end{bmatrix} \begin{Bmatrix} u_1 \\ v_1 \\ \vdots \\ u_n \\ v_n \end{Bmatrix}$$

or

$$\boldsymbol{\varepsilon} = \begin{bmatrix} \frac{\partial\phi_1}{\partial x} & 0 & \cdots & \frac{\partial\phi_n}{\partial x} & 0 \\ 0 & \frac{\partial\phi_1}{\partial y} & \cdots & 0 & \frac{\partial\phi_n}{\partial y} \\ \frac{\partial\phi_1}{\partial y} & \frac{\partial\phi_1}{\partial x} & \cdots & \frac{\partial\phi_n}{\partial y} & \frac{\partial\phi_n}{\partial x} \end{bmatrix} \begin{Bmatrix} u_1 \\ v_1 \\ \vdots \\ u_n \\ v_n \end{Bmatrix} = \mathbf{B}\mathbf{u} = \sum_I^n \mathbf{B}_I \mathbf{u}_I$$

Similarly,

$$\mathbf{L}\delta\mathbf{u}^h = \mathbf{L}\mathbf{\Phi}\delta\mathbf{u} = \mathbf{B}\delta\mathbf{u} = \sum_I^n \mathbf{B}_I \delta\mathbf{u}_I \tag{15}$$

The stress vector can be obtained using the constitutive equations.

$$\boldsymbol{\sigma} = \mathbf{D}\boldsymbol{\varepsilon} = \mathbf{B}\mathbf{D}\mathbf{u} = \sum_I^n \mathbf{D}\mathbf{B}_I \delta\mathbf{u}_I$$

where $\mathbf{B}_I$ is the strain matrix about the Ith node, $\mathbf{D}$ is the material matrix for the plane stress problem. They are given by

$$\mathbf{B}_I = \begin{bmatrix} \phi_{I,x} & 0 \\ 0 & \phi_{I,y} \\ \phi_{I,y} & \phi_{I,x} \end{bmatrix},$$

$$\mathbf{D} = \frac{E}{1-\mu^2}\begin{bmatrix} 1 & \mu & 0 \\ \mu & 1 & 0 \\ 0 & 0 & (1-\mu)/2 \end{bmatrix}$$

Substituting Equation (15) into the first term of Equation (11), we have

$$\begin{aligned} \int_\Omega (\mathbf{L}\delta\mathbf{u})^{\mathrm{T}} (\mathbf{DLu})\,\mathrm{d}\Omega &= \int_\Omega \left(\sum_I^n \mathbf{B}_I \delta\mathbf{u}_I\right)^{\mathrm{T}} \left(\sum_J^n \mathbf{DB}_J \mathbf{u}_J\right) \mathrm{d}\Omega \\ &= \int_\Omega \sum_I^n \sum_J^n \delta\mathbf{u}_I^{\mathrm{T}} \left[\mathbf{B}_I^{\mathrm{T}} \mathbf{DB}_J\right] \mathbf{u}_J \mathrm{d}\Omega \end{aligned} \tag{16}$$

Note that until this stage, I and J are based on the local numbering system for the nodes in the local support domain. We can now change the numbering system form the local one to the global one that records all the field nodes in the entire domain in a unique manner from 1 to N, the total numbering of nodes in the problem domain. Therefore, both$I$ and J in equation (16) can now vary from 1 to N .when node I and node J are not in the same local support domain, the integrand vanishes. With this operation, equation (16) can be expressed as

$$\int_\Omega (\mathbf{L}\delta\mathbf{u})^{\mathrm{T}} (\mathbf{DLu})\,\mathrm{d}\Omega = \int_\Omega \sum_I^N \sum_J^N \delta\mathbf{u}_I^{\mathrm{T}} \left[\mathbf{B}_I^{\mathrm{T}} \mathbf{DB}_J\right] \mathbf{u}_J \mathrm{d}\Omega$$

Move the integration inside the summations to arrive at

$$\int_\Omega (\mathbf{L}\delta\mathbf{u})^{\mathrm{T}} (\mathbf{DLu})\,\mathrm{d}\Omega = \sum_I^N \sum_J^N \delta\mathbf{u}_I^{\mathrm{T}} \left(\int_\Omega \left[\mathbf{B}_I^{\mathrm{T}} \mathbf{DB}_J\right] \mathrm{d}\Omega\right) \mathbf{u}_J = \sum_I^N \sum_J^N \delta\mathbf{u}_I^{\mathrm{T}} \mathbf{K}_{IJ} \mathbf{u}_J \tag{17}$$

where $\mathbf{K}_{IJ}$ is called the nodal stiffness matrix and is defined as

$$\mathbf{K}_{IJ} = \int_\Omega \mathbf{B}_I^{\mathrm{T}} \mathbf{DB}_J \mathrm{d}\Omega$$

Finally, Equation (17) becomes

$$\int_\Omega (\mathbf{L}\delta\mathbf{u})^{\mathrm{T}} (\mathbf{DLu})\,\mathrm{d}\Omega = \delta\mathbf{U}^{\mathrm{T}} \mathbf{KU} \tag{18}$$

where $\mathbf{K}$ is the global stiffness matrix in the form of

$$\mathbf{K} = \begin{bmatrix} \mathbf{K}_{11} & \mathbf{K}_{12} & \cdots & \mathbf{K}_{1N} \\ \mathbf{K}_{21} & \mathbf{K}_{22} & \cdots & \mathbf{K}_{2N} \\ \vdots & \vdots & \ddots & \vdots \\ \mathbf{K}_{N1} & \mathbf{K}_{N2} & \cdots & \mathbf{K}_{NN} \end{bmatrix}$$

In Equation (18), the vector $\mathbf{U}$ is the global displacement vector that collects the nodal displacements of all the nodes in the entire problem domain, which has the form of

$$\mathbf{U} = \begin{Bmatrix} \mathbf{u}_1 \\ \mathbf{u}_2 \\ \vdots \\ \mathbf{u}_N \end{Bmatrix} = \begin{Bmatrix} u_1 \\ v_1 \\ \vdots \\ u_N \\ v_N \end{Bmatrix}$$

Substituting Equation (14) into the second term of Equation (11), and using the same arguments in deriving the stiffness matrix, we have

$$\int_\Omega \delta \mathbf{u}^{\mathrm{T}} \mathbf{b} \mathrm{d}\Omega = \int_\Omega (\delta \sum_I^n \mathbf{\Phi}_I \mathbf{u}_I)^{\mathrm{T}} \mathbf{b} \mathrm{d}\Omega \tag{19}$$

Using the same arguments given Equation (16), Equation (19) can be expressed as

$$\int_\Omega \delta \mathbf{u}^{\mathrm{T}} \mathbf{b} \mathrm{d}\Omega = \int_\Omega (\delta \sum_I^N \mathbf{\Phi}_I \mathbf{u}_I)^{\mathrm{T}} \mathbf{b} \mathrm{d}\Omega$$

Move the integration inside the summations to arrive at

$$\int_\Omega \delta \mathbf{u}^{\mathrm{T}} \mathbf{b} \mathrm{d}\Omega = \sum_I^N \delta \mathbf{u}_I^{\mathrm{T}} \int_\Omega \mathbf{\Phi}_I^{\mathrm{T}} \mathbf{b} \mathrm{d}\Omega = \sum_I^N \delta \mathbf{u}_I^{\mathrm{T}} \mathbf{F}_I^b$$

where $\mathbf{F}_I^b$ is the nodal body force vector that is defined as

$$\mathbf{F}_I^b = \int_\Omega \mathbf{\Phi}_I^{\mathrm{T}} \mathbf{b} \mathrm{d}\Omega$$

Finally, Equation (20) becomes

$$\int_\Omega \delta \mathbf{u}^{\mathrm{T}} \mathbf{b} \mathrm{d}\Omega = \delta \mathbf{U}^{\mathrm{T}} \mathbf{F}^b \tag{20}$$

where $\mathbf{F}^b$ is the global body force vector assembled using the nodal body force vectors for all the nodes in the entire problem domain, and is defined

$$\mathbf{F}^b = \begin{Bmatrix} \mathbf{F}_1^b \\ \vdots \\ \mathbf{F}_N^b \end{Bmatrix}$$

The treatment for the last term in Equation (11) is exactly the same as that for the second term, except that the body force vector is replaced by the traction vector and the integrations are replaced by the boundary integrations. Hence, we can obtained

$$\int_{\Gamma_t} \delta \mathbf{u}^{\mathrm{T}} \bar{\mathbf{t}} \mathrm{d}\Gamma = \sum_{I}^{n} \delta \mathbf{u}_I^{\mathrm{T}} \int_{\Gamma_t} \mathbf{\Phi}_I^{\mathrm{T}} \bar{\mathbf{t}} \mathrm{d}\Gamma = \sum_{I}^{N} \delta \mathbf{u}_I^{\mathrm{T}} \int_{\Gamma_t} \mathbf{\Phi}_I^{\mathrm{T}} \bar{\mathbf{t}} \mathrm{d}\Gamma = \sum_{I}^{N} \delta \mathbf{u}_I^{\mathrm{T}} \mathbf{F}_I^t = \delta \mathbf{U}^{\mathrm{T}} \mathbf{F}^t \tag{21}$$

where $\mathbf{F}_I^t$ is the nodal traction force vector that is defined as

$$\mathbf{F}_I^t = \int_{\Gamma_t} \mathbf{\Phi}_I^{\mathrm{T}} \bar{\mathbf{t}} \mathrm{d}\Gamma$$

$\mathbf{F}^t$ is the global traction force vector assembled using the nodal traction force vectors which is defined as

$$\mathbf{F}^t = \begin{Bmatrix} \mathbf{F}_1^t \\ \vdots \\ \mathbf{F}_N^t \end{Bmatrix}$$

Substituting Equations (18), (20) and (21) into Equation (11), we can obtain

$$\delta \mathbf{U}^{\mathrm{T}} \mathbf{K} \mathbf{U} - \delta \mathbf{U}^{\mathrm{T}} \mathbf{F}^b - \delta \mathbf{U}^{\mathrm{T}} \mathbf{F}^t = 0$$

or

$$\delta \mathbf{U}^{\mathrm{T}} \left(\mathbf{K} \mathbf{U} - \mathbf{F}^b - \mathbf{F}^t \right) = 0$$

Because $\delta \mathbf{U}$ is arbitrary, the above equation can be satisfied only if

$$\mathbf{K} \mathbf{U} = \mathbf{F}^b + \mathbf{F}^t$$

It can be re-written as

$$\mathbf{K} \mathbf{U} = \mathbf{F} \tag{22}$$

where $\mathbf{F}$ is the global force vector given by

$$\mathbf{F} = \mathbf{F}^b + \mathbf{F}^t$$

Equation (22) is the final discretized system equations.

3 Formulation of the topology optimization design

3.1 The SIMP model

In SIMP model [Bendsoe and Sigmund (1999)], a penalization factor which has the effect of penalizing the intermediate density is introduced to ensure that the continuous design variables are forced towards a 0-1 solution. The relation between the density and the material tensor is written as

$$E_{ijkl}(x) = \rho^p(x) E^0_{ijkl} \tag{23}$$

where E^0_{ijkl} is the Young's modulus of a given solid material, p is a penalization factor.

The density of any point in the design domain can be interpolated by the nodal density parameters and the RPIM shape function as follow

$$\rho_g = \sum_{i=1}^{np} \mathbf{\Phi}_i \rho_i \tag{24}$$

where ρ_i is the relative density of the ith node, and is the design variable, $\mathbf{\Phi}_i$ is the RPIM shape function of the ith node, np is the number of nodes in the support domain.

Considering the relative density of the nodes as a design variable, and the minimize compliance as an objective function, the topology optimization problem based the SIMP interpolation scheme can be formulated as follows

$$\begin{aligned} &\text{find } \rho(x), \quad x \in \Omega \\ &\min\ c = \mathbf{F}^{\mathbf{T}}\mathbf{U} \\ &s.t.\ \mathbf{KU} = \mathbf{F} \\ &\quad V = \int_\Omega \rho_g \mathrm{d}\Omega = fV_0 \\ &\quad 0 < \rho_{\min} \le \rho_i \le 1 \end{aligned} \tag{25}$$

where $\mathbf{K}$ is the global stiffness matrix, $\mathbf{U}$ is the displacement vector, $\mathbf{F}$ is the force vector, V is the material volume of the design domain, V_0 is the given volume of the solid material, f is the prescribed volume fraction, $\rho_{\min}$ is a lower bound on density, introduced to prevent any possible singularity, in typical application, we set $\rho_{\min} = 0.001$.

3.2 Solution methods

The topology optimization problem could be solved using several different approaches such as Optimality Criteria (OC) method [Zhou and Rozvany (1991)],

Sequential Linear Programming (SLP) method [Fujii and Kikuchi (2000)] or the method of Moving Asymptotes (MMA) [Svanberg (1987)] and others. The OC method is simple to understand and implement, and is computationally efficient. The effectiveness of the method comes from the fact that each design variable is updated independently of the update of the other design variables. Following Sigmund(2001), a updating scheme for the design variables is formulated as follows

$$\rho_i^{new} = \begin{cases} \max(\rho_{\min}, \rho_i - m) & \text{if } \rho_i B_i^{\eta} \le \max(\rho_{\min}, \rho_i - m) \\ \rho_i B_i^{\eta} & \text{if } \max(\rho_{\min}, \rho_i - m) < \rho_i B_i^{\eta} < \min(1, \rho_i + m) \\ \min(1, \rho_i + m) & \text{if } \min(1, \rho_i + m) \le \rho_i B_i^{\eta} \end{cases} \quad (26)$$

where B_i is given by the expression

$$B_i = \frac{-\frac{\partial c}{\partial \rho_i}}{\lambda \frac{\partial V}{\partial \rho_i}}$$

where λ is a Lagrangian multiplier that can be found by a bi-sectioning algorithm, m is a positive move-limit, η is a numerical damping coefficient. The introduction m and η is to ensure the stability of the iteration.

3.3 Sensitivity analysis

We refer to the sensitivity analysis in FEM, using the adjoint method to calculate the sensitivity of the objective function.

Rewrite the objective function by adding the zero function

$$c = \mathbf{F}^{\mathrm{T}}\mathbf{U} - \tilde{\mathbf{U}}^{\mathrm{T}}(\mathbf{K}\mathbf{U} - \mathbf{F}) \quad (27)$$

where $\tilde{\mathbf{U}}$ is any arbitrary, but fixed real vector.

By the derivative of Equation (27) with respect to the design variable, we can obtain as

$$\frac{\partial c}{\partial \rho_i} = \mathbf{F}^{\mathrm{T}}\frac{\partial \mathbf{U}}{\partial \rho_i} - \tilde{\mathbf{U}}^{\mathrm{T}}\left(\frac{\partial \mathbf{K}}{\partial \rho_i}\mathbf{U} + \mathbf{K}\frac{\partial \mathbf{U}}{\partial \rho_i}\right) = \left(\mathbf{F}^{\mathrm{T}} - \tilde{\mathbf{U}}^{\mathrm{T}}\mathbf{K}\right)\frac{\partial \mathbf{U}}{\partial \rho_i} - \tilde{\mathbf{U}}^{\mathrm{T}}\frac{\partial \mathbf{K}}{\partial \rho_i}\mathbf{U} \quad (28)$$

When $\tilde{\mathbf{U}}$ satisfies the adjoint equation $\mathbf{F}^{\mathrm{T}} - \tilde{\mathbf{U}}^{\mathrm{T}}\mathbf{K} = 0$, we obtain directly that $\tilde{\mathbf{U}} = \mathbf{U}$, Equation (28) can be re-written as

$$\frac{\partial c}{\partial \rho_i} = -\mathbf{U}^{\mathrm{T}}\frac{\partial \mathbf{K}}{\partial \rho_i}\mathbf{U} \quad (29)$$

In this way the sensitivity analysis of the objective function transforms to calculate the sensitivity of the stiffness matrix with respect to the design variable.

By

$$\mathbf{K} = \int_{\Omega} \rho_g^p \mathbf{B}^{\mathrm{T}} \mathbf{D} \mathbf{B} \mathrm{d}\Omega$$

we can obtain

$$\frac{\partial \mathbf{K}}{\partial \rho_i} = \int_{\Omega} p \rho_g^{p-1} \mathbf{\Phi}_i \mathbf{B}^{\mathrm{T}} \mathbf{D} \mathbf{B} \mathrm{d}\Omega \tag{30}$$

The sensitivity of the volume constraint with respect to the design variable is obtained as follows

$$\frac{\partial V}{\partial \rho_i} = \int_{\Omega} \mathbf{\Phi}_i \mathrm{d}\Omega \tag{31}$$

4 Numerical examples

In this section, numerical examples will be given for demonstration of the feasibility and efficiency of the proposed approach.

4.1 A cantilever beam with a concentrated force applied on the middle of the free end

A cantilever beam is fixed on the left side and is loaded with a concentrated force F at the middle of the right side, as shown in Fig.1(a). The problem domain is represented by 441 field nodes, and 400 rectangular background cells are used for the numerical integrations, in each background cell 2×2 Gauss points are employed. The elastic material properties are chosen as Young's modulus $E = 3 \times 10^8$ Pa, Possion's ratio $\mu = 0.3$, and volume constraint is 50%.

The optimization result of the beam obtained by the present method is shown in Fig.1(b). For comparison, the optimization result obtained by FEM is shown in Fig.1(c) and the optimization result obtained by FEM with sensitivity filtering is shown in Fig.1(d). And the variation of the objective function with iterative number is shown in Fig.2. In the present method, the value of the objective function decreases from 0.4510 to 0.0478, and the number of iteration is 47. In FEM, the value of the objective function decreases from 0.4496 to 0.0489, and the number of iteration is 22, and in FEM with sensitivity filtering the value decreases from 0.4496 to 0.0535, and the number of iteration is 35. From these results, it can be seen that the present approach can effectively eliminate the checkerboard phenomenon arising in FEM, but the computational time increases.

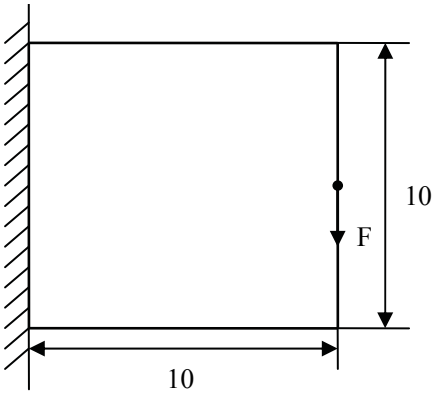

(a) Cantilever beam problem

(b) Optimization result by present method

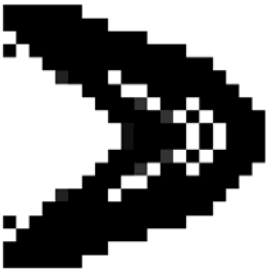

(c) Optimization result by FEM

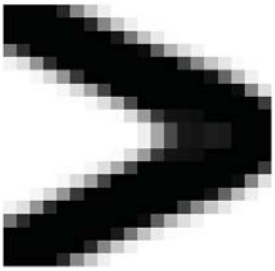

(d) Optimization result by FEM with sensitivity filtering

Figure 1

4.2 A cantilever beam with a concentrated force applied at the right lower corner

A cantilever beam is fixed on the left side and is loaded with a concentrated force F at the right lower corner, as shown in Fig.3(a). As in the previous example, the problem domain is represented by 441 field nodes, and 400 rectangular background cells are used for the numerical integrations, in each background cell 2×2 Gauss points are employed. The elastic material properties are chosen as Young's modulus $E = 3 \times 10^8$ Pa, Possion's ratio $\mu = 0.3$, and volume constraint is 40%.

The optimization result of the beam obtained by the present method is shown in Fig.3(b). The optimization result obtained by RPIM with the relative density of the

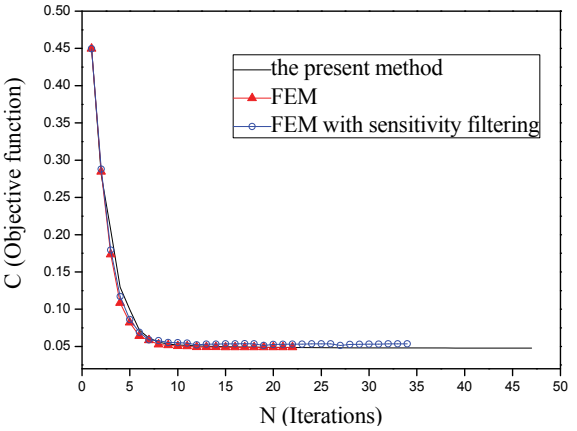

Figure 2 The variation of the objective function with iterative number

Gauss quadrature points as a design variable is shown in Fig.3(c) for comparison. And the variation of the objective function with iterative number is shown in Fig.4. In the present method, the value of the objective function decreases from 1.9150 to 0.1036, and the number of iteration is 89. In RPIM with the relative density of the Gauss quadrature points as a design variable, the value of the objective function decreases from 1.9150 to 0.0907, and the number of iteration is 59. From these results, it can be seen that the present approach can effectively eliminate the checkerboard pattern with point state arising in the latter, but the computational time increases.

5 Conclusions

In this paper, a topology optimization design is formulated using the radial point interpolation method for two-dimensional elastostatics problems. Considering the relative density of the nodes as a design variable and minimizing compliance as an objective function, the mathematical formulation of the topology optimization is developed using the SIMP interpolation scheme. The adjoint sensitivity analysis method is employed to formulate the sensitivities of the objective function and the volume constrain. Numerical examples demonstrate the proposed method can effectively eliminate the checker-board phenomenon.

Acknowledgement: This work was supported by National 973 Scientific and Technological Innovation Project (2004CB719402), Natural Science Foundation of China (No.10672055), The Key Project of NSFC of China (No.60635020) and

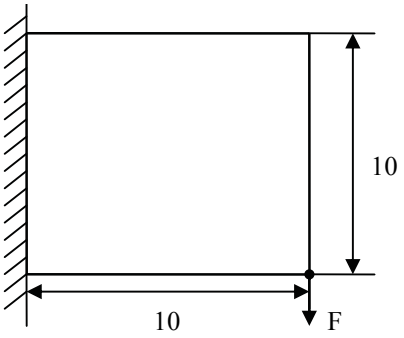

(a) Cantilever beam problem

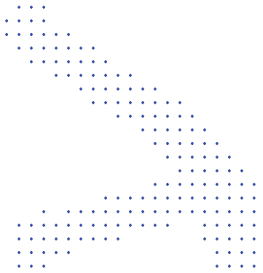

(b) Optimization result by present method

(c) Optimization result by RPIM with the densities of the Gauss quadrature points as a design variable

Figure 3

The National Science Foundation for Outstanding Youth of China (No.50625519).

References

Atluri S.N.; Zhu T. (1998): A New Meshless Local Petrov-Galerkin (MLPG) Approach in Computational Mechanics. *Computational Mechanics*, Vol.22, 117-127.

Belytschko T.; Lu Y.; Gu L. (1994): Element-free Galerkin method. *International Journal for Numerical Methods in Engineering*, 37: 229-256.

Bendsoe M.P.; Kikuchi N. (1988): Generating optimal topology in structural design using a homogenization method. *Computer Methods in Applied Mechanics and Engineering*, 71, 197-224.

Bendsoe M.P.; Sigmund O. (1999): Material interpolation schemes in topology optimization. *Archive of Applied Mechanics,* 69: 635-654.

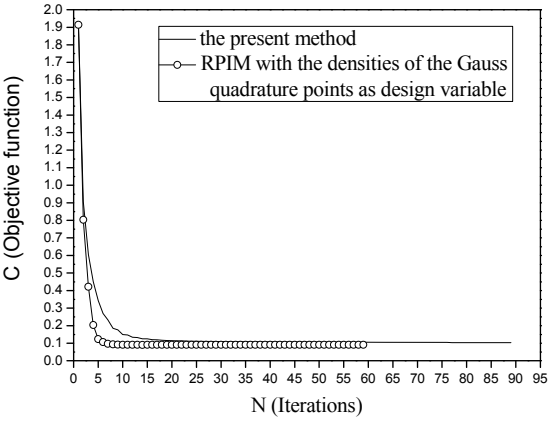

Figure 4 The variation of the objective function with iterative number

Bendsoe M.P.; Sigmund O. (2003): *Topology Optimization: Theory, Methods, and Applications.* Berlin, Heidelberg, New York: Springer.

Cisilino A.P. (2006): Topology optimization of 2D potential problems using boundary elements. *CMES: Computer Modeling in Engineering & Sciences*, Vol.15, No.2, 99-106.

Fujii D.; Kikuchi N. (2000): Improvement of numerical instabilities in topology optimization using SLP method. *Structural and Multidisciplinary Optimization*, 19, 113-121.

Li S.; Atluri S.N. (2008a): Topology optimization of structures based on the MLPG mixed collocation method. *CMES: Computer Modeling in Engineering & Sciences*, Vol.26, No.1, 61-74.

Li S.; Atluri S.N. (2008b): The MLPG Mixed Collocation Method for Material Orientation and Topology Optimization of Anisotropic Solids and Structures. *CMES: Computer Modeling in Engineering & Sciences*, Vol.30, No.1, 37-56.

Liu G.R.; Gu Y.T. (2001): A point interpolation method for two-dimensional solids. *International Journal for Numerical Methods in Engineering*, 50: 937-951.

Liu G.R.; Dai K.Y.; Lim K.M.; Gu Y.T. (2003): A radial point interpolation method for simulation of two-dimensional piezoelectric structures. *Smart Materials and Structures*, 12, 171-180.

Liu G.R.; Gu Y.T. (2004): *An Introduction to Mfree Methods and Their Programming*. Berlin, Springer Press.

Liu G.R.; Zhang G.Y.; Gu Y.T.; Wang Y.Y. (2005): A meshfree radial point inter-

polation method (RPIM) for three-dimensional solids. *Computational Mechanics*, 36: 421–430.

Liu L.; Liu G.R.; Tan V.B.C. (2002): Element free method for static and free vibration analysis of spatial thin shell structures. *Computer Methods in Applied Mechanics and Engineering*, 191, 5923–5942.

Liu W.K.; Jun S. (1995): Reproducing kernel particle methods. *International Journal for Numerical Methods in Fluids*, 20: 1081-1106.

Michael Y.W.; Wang X.M. (2004): PDE- Driven Level Sets, Shape Sensitivity and Curvature Flow for Structural Topology Optimization. *CMES: Computer Modeling in Engineering & Sciences*, Vol.6, No.4, 373- 396.

Michael Y.W.; Zhou S.W. (2004): Phase Field: A Variational Method for Structural Topology Optimization. *CMES: Computer Modeling in Engineering & Sciences*, Vol.6, No.6, 547-566.

Monaghan J.J. (1992): Smoothed particle hydrodynamics. *Annual Review of Astronomy and Astrophysics*, 30: 543-574.

Raju I.S.; Phillips D.R.; Krishnamurthy T. (2004): A radial basis function approach in the meshless local Petrov-Galerkin method for Euler-Bernoulli beam problems. *Computational Mechanics*, Vol.34, 464–474.

Sigmund O. (2001): A 99 line topology optimization code written in Matlab. *Structural and Multidiscipline Optimization*, 21(2), 120-127.

Stolpe M.; Svanberg K. (2001): An alternative interpolation scheme for minimum compliance topology optimization. *Structural and Multidiscipline Optimization*, 22, 116-124.

Svanberg K. (1987): The method of moving asymptotes: a new method for structural optimization. *International Journal for Numerical Methods in Engineering*, 24, 359-373.

Tapp C.; Hansel W.; Mittelstedt C.; Becker W. (2004): Weight-Minimization of Sandwich Structures by a Heuristic Topology Optimization Algorithm. *CMES: Computer Modeling in Engineering & Sciences*, Vol.5, No.6, 563- 574.

Wang J.G.; Liu G.R.; Lin P. (2002): Numerical analysis of Biot's consolidation process by radial point interpolation method. *International Journal of Solids and Structures*, 39(6), 1557–1573.

Wang S.Y.; Lim K.M.; Khoo B.C.; Wang M.Y. (2007a): A geometric deformation constrained level set method for structural shape and topology optimization. *CMES: Computer Modeling in Engineering & Sciences*, Vol.18, No.3, 155-181.

Wang S.Y.; Lim K.M.; Khoo B.C.; Wang M.Y. (2007b): An unconditionally time-stable level set method and its application to shape and topology optimization.

CMES: Computer Modeling in Engineering & Sciences, Vol.21, No.1, 1-40.

Wang S.Y.; Lim K.M.; Khoo B.C.; Wang M.Y. (2007c): On hole nucleation in topology optimization using the level set methods. *CMES: Computer Modeling in Engineering & Sciences*, Vol.21, No.3, 219-237.

Wang S.Y.; Lim K.M.; Khoo B.C.; Wang M.Y. (2008): A Hybrid Sensitivity Filtering Method for Topology Optimization. *CMES: Computer Modeling in Engineering & Sciences*, Vol.24, No.1, 21-50.

Wang S.Y.; Wang M.Y. (2006): Structural shape and topology optimization using an implicit free boundary parameterization method. *CMES: Computer Modeling in Engineering & Sciences*, Vol.13, No.2, 119-147.

Zhou M.; Rozvany G.I.N. (1991): The COC algorithm Part II: topological, geometry and generalized shape optimization. *Computational Methods in Applied Mechanics and Engineering*, 89, 197-224.

Zhou M.; Rozvany G.I.N. (2001): On the validity of ESO type methods in topology optimization. *Structural and Multidiscipline Optimization*, 21, 80-83.

Zhou S.; Wang M.Y. (2006): 3D multi-material structural topology optimization with the generalized Cahn-Hilliard equations. *CMES: Computer Modeling in Engineering & Sciences*, Vol.16, No.2, 83-101.